Accepted Manuscript

Photoinduced PEG deshielding from ROS-sensitive linkage-bridged block copolymer-based nanocarriers for on-demand drug delivery

Jie Li, Chunyang Sun, Wei Tao, Ziyang Cao, Haisheng Qian, Xianzhu Yang, Jun Wang

PII: S0142-9612(18)30264-3

DOI: 10.1016/j.biomaterials.2018.04.015

Reference: JBMT 18601

To appear in: *Biomaterials*

Received Date: 1 February 2018

Revised Date: 4 April 2018

Accepted Date: 9 April 2018

Please cite this article as: Li J, Sun C, Tao W, Cao Z, Qian H, Yang X, Wang J, Photoinduced PEG deshielding from ROS-sensitive linkage-bridged block copolymer-based nanocarriers for on-demand drug delivery, *Biomaterials* (2018), doi: 10.1016/j.biomaterials.2018.04.015.

Photoinduced PEG Deshielding from ROS-Sensitive Linkage-Bridged Block Copolymer-based Nanocarriers for On-Demand Drug Delivery

Jie Li[a,§], Chunyang Sun[b,§], Wei Tao[a,§], Ziyang Cao[a], Haisheng Qian[a], Xianzhu Yang,[a,c,d]* and Jun Wang[c,d,f,]*

[a] School of Biological and Medical Engineering, Hefei University of Technology, Hefei, Anhui 230009, P.R. China

[b] Department of Radiology and Tianjin Key Laboratory of Functional Imaging, Tianjin Medical University General Hospital, Tianjin 300052, P.R. China

[c] Institutes for Life Sciences, School of Medicine, South China University of Technology, Guangzhou, Guangdong 510006, China

[d] National Engineering Research Center for Tissue Restoration and Reconstruction, South China University of Technology, Guangzhou, Guangdong 510006, P.R. China

[f] Guangdong Key Laboratory of Nanomedicine, Shenzhen Institutes of Advanced Technology, Chinese Academy of Sciences, Shenzhen 518055, China

[§] These authors contribute equally to this work.

***Corresponding Authors:** Xianzhu Yang, E-mail: yangxz@scut.edu.cn; Jun Wang, E-mail: mcjwang@scut.edu.cn;

ABSTRACT: Controlling poly(ethylene glycol) (PEG) shielding/deshielding at the desired site of action exhibits great advantages for nanocarrier-based on-demand drug delivery *in vivo*. However, the current PEG deshielding strategies were mainly designed for anticancer drug delivery; even so, their applications are also limited by tumor heterogeneity. As a proof-of-concept, we explored a photoinduced PEG deshielding nanocarrier TK-$NP_{Ce6\&PTX}$ to circumvent the aforementioned challenge. The TK-$NP_{Ce6\&PTX}$ encapsulating chlorin e6 (Ce6) and paclitaxel (PTX) was self-assembled from an innovative thioketal (TK) linkage-bridged diblock copolymer of PEG with poly(d,l-lactic acid) (PEG-*TK*-PLA). We demonstrated that the high PEGylation of TK-$NP_{Ce6\&PTX}$ in blood helps the nanocarrier efficiently avoid rapid clearance and consequently prolongs its circulation time. At the desired site (tumor), 660-nm red light irradiation led to ROS generation *in situ*, which readily cleaved the TK linkage, resulting in PEG deshielding. Such photoinduced PEG deshielding at the desired site significantly enhances the cellular uptake of the nanocarriers, achieving on-demand drug delivery and superior therapeutic efficacy. More importantly, this strategy of photoinducing PEG deshielding of nanocarriers could potentially extend to a variety of therapeutic agents beyond anticancer drugs for on-demand delivery.

Keywords: PEG deshielding, ROS-sensitive block copolymer, on-demand drug delivery, photocontrolled drug delivery, PEG-dilemma

1. Introduction

Polyethylene glycol (PEG) has been widely used to modify nanocarriers to reduce the non-specific cellular uptake of drug delivery vehicles *in vivo*,[1-4] which consequently prolongs the circulation time and decreases the cytotoxicity to normal healthy tissues or organs.[5-8] Several PEGylated nanocarriers, including Doxil and Genexol-PM, have been approved for clinical use, and nearly ten pioneering clinical trials of nanocarrier-based therapies are ongoing.[9-11] However, the PEGylation also inhibits the internalization of nanocarriers into target cells and further limits the therapeutic efficiency (known as the PEG dilemma).[12-14] To circumvent this dilemma, various smart "sheddable" nanocarriers have recently been explored by scientists, in which the PEG can be deshielded from the nanocarriers in the target tissue to significantly promote cellular uptake and subsequently improve drug delivery efficiency.[15-18] For the current sheddable nanocarriers, PEG deshielding was mainly achieved by responding to the local stimuli of the tumor microenviroment, such as a slightly acidic tumor microenvironment and various overexpressed enzymes.[19-22] It should be noted that, for the tumor acidity-responsive formulations, the PEG segment was also deshielded in the blood circulation at a relatively lower rate compared to the rate in the slightly acidic tumor tissue.[19] For the enzyme-responsive formulations, the expressions of these enzymes in different tumor patients or in the same individual at different tumor stages were dynamically changed,[23,24] which could lead to varied PEG shielding effects and, hereafter uncontrollable anticancer efficacy. More importantly, these sheddable nanocarriers, which were designed to circumvent the PEG-dilemma for anticancer drug delivery, cannot be extended to deliver therapeutice agents to other desired tissues.[25] Thus, exploring alternative strategies with precisely controlled PEG deshielding capability to any desired site, not just tumor cells, is urgently needed.

Recently, light has been widely utilized as an attractive external stimulus, which can be remotely manipulated with high spatial and temporal resolutions, to fabricate smart nanocarriers for on-demand drug delivery and drug release.[26,27] Specifically, red or near-infrared (NIR) light with wavelengths in the range of approximately 650-950 nm, is suitable for biomedical applications because of its greater tissue penetration, reduced scattering, and minimal phototoxicity.[28,29] Consequently, red and NIR light seem to be a perfect stimulus to induce PEG shielding in the desired tissue to enhance drug delivery efficacy. Unfortunately, the low energy of the red and NIR light directly resulted in inefficient cleaving of the chemical bond.[30,31] Realizing the photoinduced PEG shielding from the nanocarriers remains a major challenge.

Recent reports have demonstrated that the thioketal (TK) bond can be readily cleaved by reactive oxygen species (ROS).[32-34] ROS is capable of being generated specifically by photosensitizers under red or NIR light irradiation. In light of this, an innovative TK linkage-bridged diblock copolymer of PEG with polylactide (PLA) (PEG-*TK*-PLA) was synthesized and used to encapsulate the photosensitizer Ce6 and the chemotherapeutic drug PTX (TK-$NP_{Ce6\&PTX}$, Scheme 1). At the target tissue, 660-nm red light irradiation efficiently produced ROS by the encapsulated Ce6 to rapidly degrade the TK linkage *in situ*; consequently, the PEG corona of TK-$NP_{Ce6\&PTX}$ rapidly deshielded, which significantly enhanced the cellular uptake. We systematically and comprehensively evaluated the effect of the photoinduced PEG deshielding of TK-$NP_{Ce6\&PTX}$ on the nanocarrier's circulation, internalization, accumulation, and overall antitumor efficacy. This study provides new avenues for the fabrication of PEG sheddable nanocarriers for on-demand drug delivery.

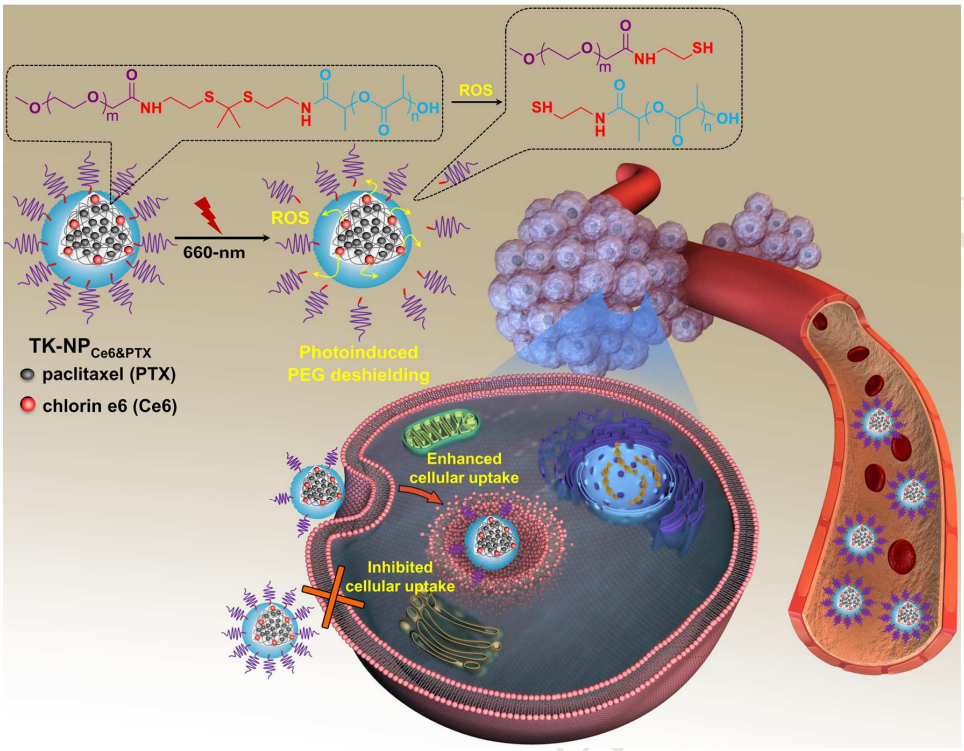

Scheme 1. Schematic illustration of the ROS-sensitive linkage-bridged diblock copolymer-based nanocarriers TK-$NP_{Ce6\&PTX}$ for on-demand drug delivery by photoinduced PEG deshielding. Without NIR irradiation, the PEGylation of TK-$NP_{Ce6\&PTX}$ avoided rapid clearance and prolonged its circulation time. At the tumor site, the encapsulated Ce6 under 660-nm red light irradiation efficiently produced ROS to rapidly degrade the TK linkage *in situ*, resulting in PEG deshielding and consequently enhanced cellular uptake.

2. Materials and methods

Materials. PTX, 3-(4,5-Dimethylthiazol-2-yl)-2,5-diphenyl tetrazolium bromide (MTT) and 4,6-diamidino-2-phenylindole (DAPI) were purchased from Sigma-Aldrich (St. Louis, USA). Chlorin e6 (Ce6) was purchased from Shanghai New Union Textra Import & Export Co., Ltd. (Shanghai, China). Dulbecco's-modified eagle medium (DMEM) and fetal bovine serum (FBS)

were purchased from Gibco BRL (Eggenstein, Germany). Methoxy and carboxyl terminated PEG (Mn=5,000) were purchased from Aladdin Chemical Co., Ltd. (Shanghai, China). D,L-lactide was purchased from Jinan Daigang Biomaterial Co. Ltd. (China). FITC-labeled PLA (Mn=1.0×10^4) was purchased from Xi'an Ruixi Biological Technology Co., Ltd. (Xi'an, China). The synthesis processes of $mPEG_{113}$-*TK*-PLA_{140} and $mPEG_{113}$-*b*-PLA_{142} was described in the supporting information. Other organic solvents and reagents were used as received.

Characterizations. NMR spectra were recorded in deuterated reagent with an Agilent VNMRS 600 MHz NMR spectrometer (California, USA). The molecular weights of the samples were measured on a Waters gel permeation chromatography (GPC) system.[35] The size of the nanocarriers was measured by DLS (NanoBrook-90 Plus instrument, Brookhaven Instrument Corporation, Holtsville, New York, USA). The morphology of the nanoparticles was analyzed by JEM-2100F transmission electron microscopy (TEM) at an accelerating voltage of 200 kV. The concentrations of PTX and Ce6 were determined by an HPLC method and UV-Vis spectroscopy, as previously reported.[21,36]

Preparation of TK-$NP_{Ce6\&PTX}$ and $NP_{Ce6\&PTX}$. To prepare TK-$NP_{Ce6\&PTX}$, Ce6 (0.2 mg), PTX (1.0 mg) and $mPEG_{113}$-*TK*-PLA_{140} (10.0 mg) were dissolved in dimethyl sulfoxide (DMSO, 1.0 mL) for 30 min, and then water (10.0 mL) was added dropwise and continually stirred for another 4 h. Thereafter, the mixture solution was transferred to a dialysis tube (cutoff molecular weight was 14,000 Da) to remove the DMSO. The final solution was filtered through a 0.45 μm filter (Millipore). $NP_{Ce6\&PTX}$ was similarly prepared by replacing $mPEG_{113}$-*TK*-PLA_{140} with $mPEG_{113}$-*b*-PLA_{142}. Similarly, the FITC-labeled nanocarriers ^{FITC}TK-$NP_{Ce6\&PTX}$ and $^{FITC}NP_{Ce6\&PTX}$ were prepared by adding FITC-labeled PLA (0.2 mg) during the procedure.

PEG deshielding of TK-NP$_{Ce6\&PTX}$ under 660-nm light. The solution of TK-NP$_{Ce6\&PTX}$ (1.0 mg/mL, 10 mL) in a centrifuge tube was immersed in a water bath at 37 °C and then irradiated with 660-nm red light (0.2 W/cm^2) for different times. Subsequently, partial samples were collected and lyophilized for GPC analysis, and other samples were collected by centrifugation (100,000 × g, 1 h). The concentration of the resultant thiol-terminated PEG in the supernatant was determined by Ellman's reagent DTNB according to the previously reported method.[27] In addition, the ROS generation was determined according to previously reported method.[36]

Additionally, the solution of TK-NP$_{Ce6\&PTX}$ and NP$_{Ce6\&PTX}$ (1.0 mg/mL, 1.0 mL) in a centrifuge tube was immersed in a water bath at 37 °C and was then exposed to 660-nm red light (0.2 W/cm^2, 30 min). Thereafter, the size distributions and morphologies of both samples with or without light irradiation were detected by DLS and TEM, respectively. Meanwhile, the samples were suspended in a PBS containing 10% FBS, and the size changes were monitored by DLS after incubation for different time periods.

In addition, after preirradiation (660 nm, 0.2 W/cm^2, 30 min), the TK-NP$_{Ce6\&PTX}$ or NP$_{Ce6\&PTX}$ (1.0 mg/mL, 1.0 mL) was transferred into the dialysis membrane tubing and was then immersed in the PB buffer (0.02 M, pH 7.4, 15 mL) at 37 °C. Then, the release of PTX was determined using HPLC analysis, as previously reported.[37]

The cellular uptake of TK-NP$_{Ce6\&PTX}$ preirradiated with 660-nm light. After light preirradiation (660 nm, 0.2 W/cm^2, 10 min or 30 min), the FITC-labeled nanocarriers ^{FITC}TK-NP$_{Ce6\&PTX}$ or ^{FITC}NP$_{Ce6\&PTX}$ (1.0 mg/mL, 0.1 mL) were separately added into the culture medium (0.5 mL) of MDA-MB-231 cells in 24-well plates. ^{FITC}TK-NP$_{Ce6\&PTX}$ and ^{FITC}NP$_{Ce6\&PTX}$ without preirradiation were used as the controls. After incubation for 2 h or 4 h, the MDA-MB-231 cells were washed twice, trypsinized, collected, and subjected to FACS analyses on a BD FACS

Calibur flow cytometer (BD Bioscience, Bedford, MA, USA). In addition, the partial samples were lyophilized to determine the intracellular concentration of PTX by HPLC analysis.

For CLSM observations, the ^{FITC}TK-NP$_{Ce6\&PTX}$ and ^{FITC}NP$_{Ce6\&PTX}$ were preirradiated and then co-incubated with MDA-MB-231 cells, as described above. After incubating for 4 h, the cells were counterstained with DAPI and Alexa Fluor568 phalloidin according to the protocols provided by the manufacturers and were then observed by CLSM (LSM 710, Carl Zeiss, Inc., Jena, Germany).

***In vitro* cytotoxicity and apoptosis assay.** TK-NP$_{Ce6\&PTX}$ and NP$_{Ce6\&PTX}$ were preirradiated as described above and were then co-incubated with MDA-MB-231 cells at different concentrations. After incubating for 4 h, non-internalized nanocarriers were removed, and the MDA-MB-231 cell viabilities were measured by MTT assay after further incubation for 24 h. In addition, the cells, which were treated with these samples at a PTX concentration of 4.0 μg/mL, were stained with the Annexin V-FITC apoptosis detection kit I (BD Biosciences) according to the protocols provided by the manufacturers to determine the cell apoptosis rate.

Animal and tumor model. Female BALB/c nude mice and ICR mice were purchased from Beijing HFK Bioscience Co. Ltd. To establish a cancer xenograft tumor model, MDA-MB-231 cells (2×10^6) cells were injected into the mammary fat pads of female BALB/c nude mice. After the tumor volumes reached 50 mm^3, the mice were used for subsequent experiments. All mice received care in compliance with the guidelines outlined in the Guide for the Care and Use of Laboratory Animals. The procedures were approved by the Hefei University of Technology Animal Care and Use Committee.

Pharmacokinetic studies. ICR mice were randomly divided into three groups (n=4 per group) and were intravenously injected with 200 μL of TK-NP$_{Ce6\&PTX}$, NP$_{Ce6\&PTX}$, and free PTX

(dissolved in 1% DMSO) at an equivalent PTX dose of 10.0 mg/kg. At the predetermined times, blood samples were collected, and 100 μL of plasma were obtained. To determine the PTX concentration, 200 μL of acetonitrile was added to the collected plasma and vortexed for 5 min. Then, the samples were centrifuged at 10,000 × g for 10 min. The PTX concentration in the supernatant was measured by HPLC.

PTX distribution in major organs and tumor tissue. Mice bearing MDA-MB-231 tumors were intravenously injected with ^{FITC}TK-NP$_{Ce6\&PTX}$ or ^{FITC}NP$_{Ce6\&PTX}$ at an equivalent PTX injection dose of 10.0 mg/kg. At 2 h post-injection, the tumors sites of partial mice were irradiated with 660-nm light (0.2 W/cm^2, 30 min). Thereafter, at 6 h or 24 h post-injection, the tumor tissue and main organs were collected from the sacrificed mice. Subsequently, the PTX content in the tumor tissue was quantified using HPLC, and the accumulation of both FITC-labeled nanocarriers in the tumor and main organs was visualized using a Xenogen IVIS® Lumina system.

***In vivo* antitumor efficacy.** Mice bearing MDA-MB-231 tumors were intravenous injected with 200 μL of TK-NP$_{Ce6\&PTX}$, NP$_{Ce6\&PTX}$, or free PTX at an equivalent PTX injection dose of 2.5 mg/kg. At 2 h post-injection, the tumors sites were irradiated by 660 nm light (0.2 W/cm^2, 30 min). Mice without irradiation were used as controls. The mice received the treatments described above once a week. The estimated tumor volume was monitored by measuring the perpendicular diameters of the tumors and was then calculated according to the formula: tumor volume (mm^3) = 0.5 × length × width^2. The weight of each mouse was also measured every three days.

Immunohistochemical Analysis. After the last measurement, the tumor tissues were excised from the sacrificed mice and weighed. Then, these tissues were fixed in 4% formaldehyde and

embedded in paraffin for immunohistochemical staining of the proliferating cell nuclear antigen (PCNA) and the terminal transferase dUTP nick-end labeling (TUNEL) assay.

Statistical Analysis. The statistical significance of treatment outcomes was assessed using a Student's t-test; *p values < 0.05, **p values < 0.01, and ***p values < 0.005 were considered statistically significant in all analyses.

3. Results and Discussion

To synthesize the TK linkage-bridged diblock copolymer mPEG-*TK*-PLA, ROS-cleavable 2,2'-(propane-2,2-diylbis(sulfanediyl))bis(ethan-1-amine) (PDSE, Figure S1) was first reacted with carboxyl-terminated PEG to obtain $mPEG_{113}$-*TK* (Scheme S1), and its structure was confirmed by ^{1}H NMR (Figure 1A). Subsequently, the $mPEG_{113}$-*TK* was used as a macroinitiator in the second step for the ring-opening polymerization of D,L-lactide. The successful synthesis of $mPEG_{113}$-*TK*-PLA_{140} was verified using ^{1}H NMR spectroscopy (Figure 1A). The average degrees of polymerization (DP) of PLA block was 140, which was calculated by comparisons of the integrals of methylene proton resonances of PEG backbone (3.70 ppm) to methine protons of PLA backbone (1.57 ppm). Meanwhile, the ROS-insensitive diblock copolymer $mPEG_{113}$-*b*-PLA_{142} was also successfully synthesized as a control (Figure S2). The successful synthesis of $mPEG_{113}$-*TK*-PLA_{140} and $mPEG_{113}$-*b*-PLA_{142} were also verified using GPC (Figure 1B), which indicated that both diblock polymers exhibited unimodal peaks toward higher molecular weights compared with the macroinitiator $mPEG_{113}$ or $mPEG_{113}$-*TK*.

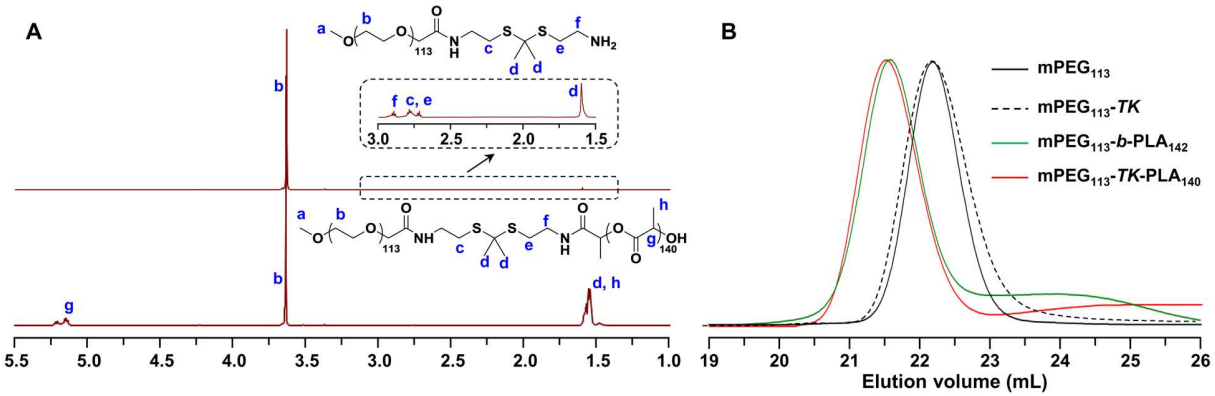

Figure 1. (A) ^{1}H NMR spectra of the macroinitiator mPEG$_{113}$-TK and mPEG$_{113}$-*TK*-PLA$_{140}$. The subscript numbers represent the DP of PEG or PLA block. (B) GPC spectra of the macroinitiator mPEG$_{113}$, mPEG$_{113}$-*TK*, mPEG$_{113}$-*TK*-PLA$_{140}$ and mPEG$_{113}$-*b*-PLA$_{142}$.

Thereafter, the obtained amphiphilic polymer mPEG-*TK*-PLA was used to simultaneously encapsulate Ce6 and PTX by the nanoprecipitation method, and the obtained nanocarrier was denoted as TK-NP$_{Ce6\&PTX}$. The loading contents of Ce6 and PTX for TK-NP$_{Ce6\&PTX}$ were approximately 0.62±0.11% and 4.88±0.31%, respectively. Additionally, the Ce6 and PTX co-loaded nanocarriers NP$_{Ce6\&PTX}$ exhibited similar loading contents, reaching 0.63±0.09% and 4.79±0.26%, respectively.

According to our design, the 660-nm red light irradiation would produce ROS by the encapsulated Ce6 to efficiently cleave the TK linkages, resulting in the PEG shielding. To demonstrate this, the TK-NP$_{Ce6\&PTX}$ and NP$_{Ce6\&PTX}$ were exposed to 660-nm light at a power density of 0.2 W/cm^2 for different periods, and then nanocarriers were collected and lyophilized for GPC analysis. It was observed that the shoulder peak gradually emerged at 22.2 min (Figure 2A), and its intensity increased as the irradiation time increased. To quantitatively determine the PEG shielding, the TK-NP$_{Ce6\&PTX}$ and NP$_{Ce6\&PTX}$ were exposed to a 660-nm laser as described above, and then the nanocarriers were collected by centrifugation (100,000 × g, 1 h), the

concentration of resultant thiol-terminated PEG in the supernatant was determined to calculate the degradation ratios of $mPEG_{113}$-*TK*-PLA_{140} and $mPEG_{113}$-*b*-PLA_{142}. As shown in Figure 2B, the degradation ratios of the mPEG-*TK*-PLA gradually increased, which was consistent with the result of Figure 2A; after 10 min and 30 min irradiations, approximately 24.4% and 50.3% of the PEG segment were efficiently deshielded from the TK-$NP_{Ce6\&PTX}$, respectively. In contrast, the degradation of PEG-*b*-PLA was negligible. In addition, the collected precipitation of TK-$NP_{Ce6\&PTX}$ was lyophilized and analyzed by ^{1}H NMR. As shown in Figure 2C, the peak at 3.70 ppm (the methylene proton resonances of PEG backbone) gradually decreased as the irradiation time increased. It should be noted that TK-$NP_{Ce6\&PTX}$ and $NP_{Ce6\&PTX}$ produced comparable ROS under the 660-nm light irradiation (Figure S3). Based on these results, it could be concluded that the PEG deshielding of TK-$NP_{Ce6\&PTX}$ was efficiently achieved under 660-nm light.

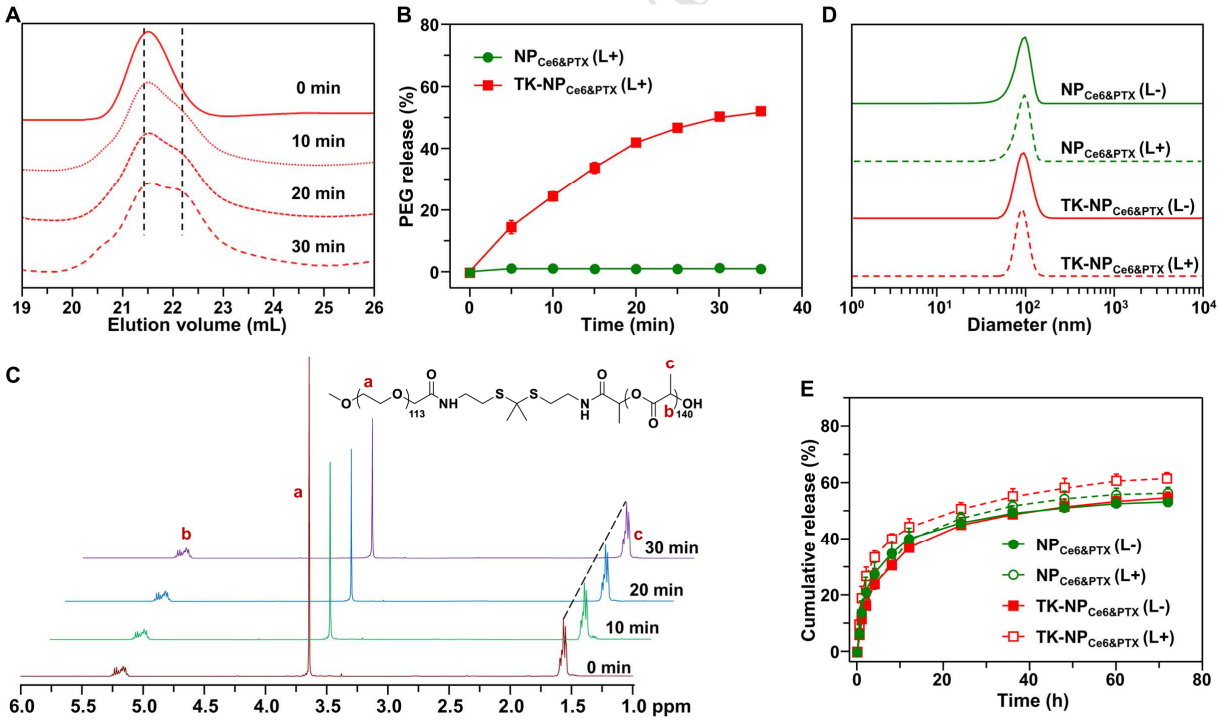

Figure 2. The PEG deshielding from TK-$NP_{Ce6\&PTX}$ under a 660-nm laser. (A) GPC measurements of TK-$NP_{Ce6\&PTX}$ with 660-nm light irradiation for 10 min, 20 min, and 30 min.

TK-$NP_{Ce6\&PTX}$ without light irradiation was used as a control. (B) The PEG deshielding ratios *versus* irradiation times for TK-$NP_{Ce6\&PTX}$ and $NP_{Ce6\&PTX}$. (C) ^{1}H NMR spectra of collected precipitation from TK-$NP_{Ce6\&PTX}$ with 660-nm light irradiation for different times (0, 10, 20, and 30 min) at a power density of 0.2 W/cm^2. (D, E) Size distributions (D) and PTX release (E) of TK-$NP_{Ce6\&PTX}$ with (L+) or without (L-) 660-nm light irradiation. The $NP_{Ce6\&PTX}$ was used as a control.

Thereafter, the size, stability, morphology, and PTX release profile of TK-$NP_{Ce6\&PTX}$ and $NP_{Ce6\&PTX}$ with or without 660 nm light irradiation (0.2 W/cm^2, 30 min) were also determined. It was observed that the photoinduced PEG deshielding did not affect their size and morphologies; the sizes of TK-$NP_{Ce6\&PTX}$ and $NP_{Ce6\&PTX}$ as measured by dynamic light scattering (DLS) were approximately similar at 100 nm (Figure 2D), and the morphologies of these nanocarriers exhibited compact and spherical morphologies (Figure S4). After PEG deshielding, the PTX release from TK-$NP_{Ce6\&PTX}$(L+) only slightly increased compared to that without the 660-nm light irradiation (Figure 2E). In addition, the TK-$NP_{Ce6\&PTX}$(L+) group also maintained its diameter for over 60 h (Figure S5), which could mean that the residual PEG was also capable of stabilizing the nanocarrier TK-$NP_{Ce6\&PTX}$.

According to our design, photoinduced PEG deshielding should enhance the cellular uptake of the nanocarriers. To confirm this hypothesis, the cellular uptake of TK-$NP_{Ce6\&PTX}$ with or without 660-nm light irradiation was investigated. The fluorescein isothiocyanate (FITC)-labeled TK-$NP_{Ce6\&PTX}$ (^{FITC}TK-$NP_{Ce6\&PTX}$) or $NP_{Ce6\&PTX}$ ($^{FITC}NP_{Ce6\&PTX}$) was exposed to 660-nm light irradiation at a density of 0.2 W/cm^2 for 10 min or 30 min and was then co-incubated with MDA-MB-231 cells for 4 h. Thereafter, intracellular FITC fluorescence was determined by flow cytometric analysis. As shown in Figure 3A, the cells incubated with ^{FITC}TK-$NP_{Ce6\&PTX}$ plus

660-nm light irradiation exhibited much stronger intracellular FITC fluorescence than cells that did not receive light irradiation, and the intracellular FITC fluorescence intensity increased as the irradiation time increased. Because approximately 24.4% and 50.3% of the PEG were efficiently deshielded from TK-$NP_{Ce6\&PTX}$ following 660-nm light irradiation for 10 min and 30 min, respectively, as described above (Figure 2B). Additionally, the changes of PEG density for TK-$NP_{Ce6\&PTX}$ after 660-nm light irradiation (0.2 W/cm^2, 10 min or 30 min) were calculated according to previously reported methods.[38] Based on the the ^{1}H NMR (Figure S6) and equation (supporting information), it could be calculated that the PEG density of TK-$NP_{Ce6\&PTX}$ decreased from 0.77 to 0.62 or 0.34 PEG/nm^2, respectively. Such reducing surface PEG density was sufficient to increase cellular uptake of nanocarrier, which has been widely reported.[6, 39] Since the cellular uptake of nanoparticles is dependent on surface PEG density, and high surface PEG density made the nanoparticles resistant to cellular uptake.[40, 41] Such enhanced cellular uptake under 660-nm light irradiation was not observed in cells treated with $^{FITC}NP_{Ce6\&PTX}$ (Figure 3B) because the photoinduced PEG deshielding cannot be realized for $NP_{Ce6\&PTX}$.

On the other hand, the enhanced tumor cell uptake under 660-nm light irradiation was further corroborated by confocal laser scanning microscopy (CLSM). The ^{FITC}TK-$NP_{Ce6\&PTX}$ and $^{FITC}NP_{Ce6\&PTX}$ were preirradiated and then co-incubated with MDA-MB-231 cells as described above. As shown in Figure S7, the cellular uptake of $^{FITC}NP_{Ce6\&PTX}$ was not affected by 660-nm light irradiation, while a much stronger cellular green fluorescence for ^{FITC}TK-$NP_{Ce6\&PTX}$ preirradiated with 660-nm light irradiation for either 10 min or 30 min was clearly observed when compared to cells treated with $^{FITC}NP_{Ce6\&PTX}$ without light preirradiation (Figure 3C).

Moreover, the TK-$NP_{Ce6\&PTX}$ or $NP_{Ce6\&PTX}$ was preirradiated with 660-nm light for different periods and then co-incubated with tumor cells for 2 h or 4 h. Subsequently, the cells were

collected, and the intracellular PTX concentration was quantitatively determined. For the TK-$NP_{Ce6\&PTX}$ group, 660-nm light irradiations of 10 min and 30 min significantly improved the amount of intracellular PTX at both time points (Figure 3D). For instance, after a 4 h incubation, the 660 nm preirradiation of 10 min and 30 min resulted in amounts of intracellular PTX approximately 1.39 and 2.34 times higher than those in cells treated with TK-$NP_{Ce6\&PTX}$ without light preirradiation. In contrast, 660 nm preirradiation did not affect the amount of intracellular PTX when the MDA-MB-231 was incubated with $NP_{Ce6\&PTX}$ at both time points. Thus, these results demonstrated that the photoinduced PEG deshielding effect resulted in enhanced tumor cell uptake of TK-$NP_{Ce6\&PTX}$.

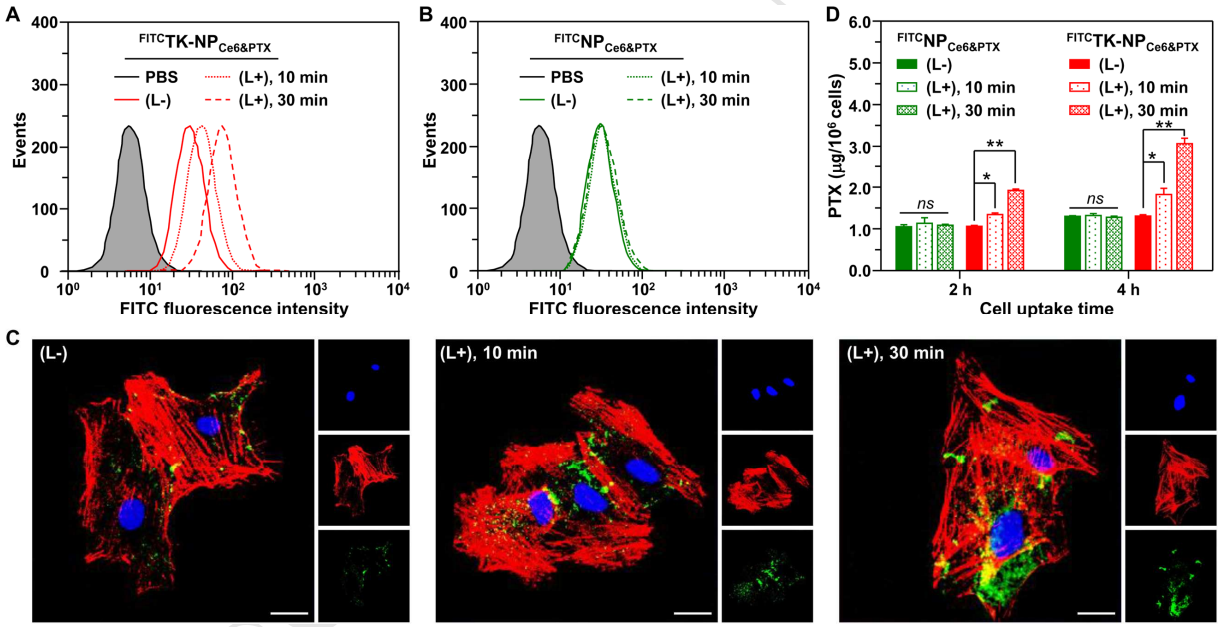

Figure 3. Photoinduced PEG deshielding for enhanced cellular uptake. The FITC-labeled ^{FITC}TK-$NP_{Ce6\&PTX}$ and $^{FITC}NP_{Ce6\&PTX}$ were preirradiated under 660-nm red light (L+, 0.2 W/cm^2) for 10 min or 30 min. Both nanoparticles without light preirradiation (L-) were used as a control. (A, B) Flow cytometric analyses of MDA-MB-231 cells after incubation with ^{FITC}TK-$NP_{Ce6\&PTX}$(L+) (A) and $^{FITC}NP_{Ce6\&PTX}$(L+) (B). (C) CLSM images of ^{FITC}TK-$NP_{Ce6\&PTX}$(L+) in

MDA-MB-231 cells. The scale bar was 10 μm. The cell nuclei and F-actin were counterstained with DAPI (blue) and Alexa Fluor568 phalloidin (red), respectively. (D) HPLC quantitative analyses of the intracellular PTX concentrations after treatment as described in (A) and (B). *p < 0.05, **p < 0.01.

The increased amount of intracellular PTX by TK-$NP_{Ce6\&PTX}$ under 660-nm light irradiation would result in enhanced anti-proliferation activity of cancer cells. To demonstrate this, the TK-$NP_{Ce6\&PTX}$ was preirradiated with or without 660 nm lasers (0.2 W/cm^2, 30 min) and was then incubated with MDA-MB-231 cells for 4 h. After removing the non-internalized nanocarriers and further incubating in a fresh medium for 24 h, the MDA-MB-231 cell viability was detected by an MTT assay (Figure 4A). At each concentration, it could be clearly observed that more tumor cells were destroyed by TK-$NP_{Ce6\&PTX}$ plus light preirradiation (TK-$NP_{Ce6\&PTX}$(L+)) compared to those without light preirradiation (TK-$NP_{Ce6\&PTX}$(L-)), exhibiting the highest efficacies for inhibiting tumor cell growth. In contrast, 660-nm light preirradiation did not improve the cytotoxicity of $NP_{Ce6\&PTX}$ to MDA-MB-231 cells.

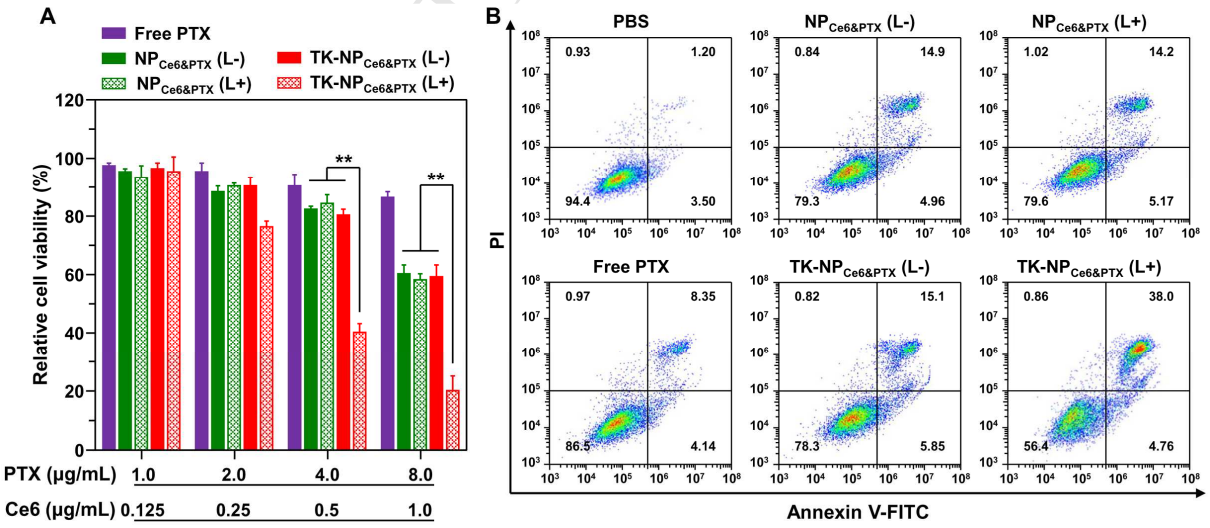

Figure 4. The photoinduced PEG deshielding significantly enhanced the anticancer efficacy *in vitro*. (A) The relative cell viabilities of MDA-MB-231 cells after treatment with TK-$NP_{Ce6\&PTX}$(L+) and $NP_{Ce6\&PTX}$(L+). The TK-$NP_{Ce6\&PTX}$(L+) and $NP_{Ce6\&PTX}$(L+) represented preirradiation with 660-nm light irradiation (0.2 W/cm^2, 30 min) before co-incubation with cells. Both nanoparticles without light irradiation, TK-$NP_{Ce6\&PTX}$(L-) and $NP_{Ce6\&PTX}$(L-), were used as controls. $^{**}p < 0.01$. (B) Flow cytometric analysis of MDA-MB-231 cell apoptosis induced by different treatments at an equivalent PTX concentration of 4.0 μg/mL.

Furthermore, the cell apoptosis was also detected. After treatment as mentioned above at an equivalent PTX concentration of 4.0 μg/mL, the MDA-MB-231 cells were stained with Annexin-V-FITC and propidium iodide (PI). As shown in Figure 4B, TK-$NP_{Ce6\&PTX}$(L-) and $NP_{Ce6\&PTX}$(L-) induced apoptosis in 19.86% and 20.95% of the MDA-MB-231 cells. Pre-irradiating $NP_{Ce6\&PTX}$ with 660-nm light irradiation did not elevate cell apoptosis (19.37%). In contrast, treatment with TK-$NP_{Ce6\&PTX}$(L+) induced 42.76% cell apoptosis, which was the highest apoptotic ratio among these treatments. Thus, these anticancer results demonstrated that the photoinduced PEG deshielding effect remarkable elevated the nanocarrier's efficacy in destroying tumor cells.

Encouraged by the superior efficacy of TK-$NP_{Ce6\&PTX}$(L+) *in vitro*, the *in vivo* animal experiment was performed to demonstrate the advantage of photoinduced PEG deshielding for nanocarriers-based cancer therapy. The mice were intravenously injected with TK-$NP_{Ce6\&PTX}$, $NP_{Ce6\&PTX}$, or free PTX, and the concentrations of PTX versus time were determined using HPLC. As shown in Figure 5A, TK-$NP_{Ce6\&PTX}$ and $NP_{Ce6\&PTX}$, which both contained high levels of PEGylation, exhibited a prolonged circulation time in the blood compared with those of free PTX. Furthermore, the pharmacokinetic parameters of these formulations were calculated (Table

S1). It was observed that the PEGylation of TK-$NP_{Ce6\&PTX}$ and $NP_{Ce6\&PTX}$ ensured large areas under the curve (AUC) compared to that of the free PTX, being 15.5-fold and 18.0-fold greater than that of free PTX. In addition, the high PEGylation also induced a much slower blood clearance rate of TK-$NP_{Ce6\&PTX}$ and $NP_{Ce6\&PTX}$ than that of free PTX. Overall, we concluded that TK-$NP_{Ce6\&PTX}$ and $NP_{Ce6\&PTX}$ exhibited remarkably prolonged circulation times, which was to the high PEGylation of nanocarriers that minimized their recognition by MPS cells during circulation and consequently helped them avoid rapid clearance by the RES.

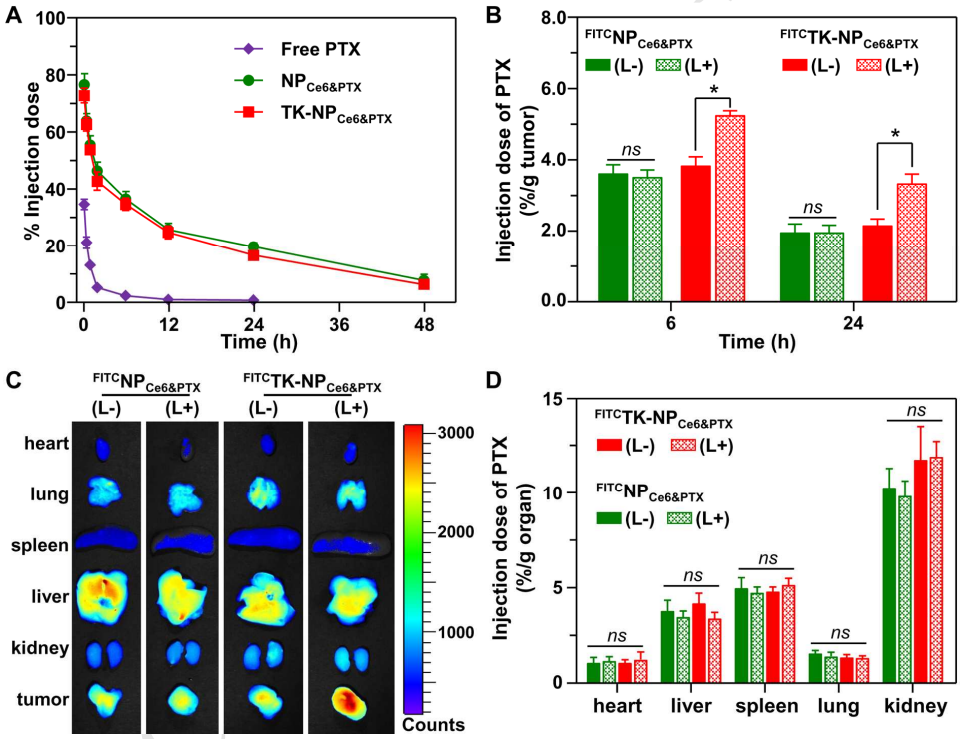

Figure 5. Photoinduced PEG deshielding for enhanced tumor accumulation *in vivo*. (A) Plasma PTX concentration *versus* time after intravenous injection of free PTX in 1% DMSO, TK-$NP_{Ce6\&PTX}$, and $NP_{Ce6\&PTX}$. (B) The quantification of PTX contents in tumor tissue by HPLC. *p < 0.05. (C) *Ex vivo* images of heart, lung, spleen, liver, kidney, and tumor tissue at 24 h post-injection. (D) The quantification of the PTX contents in major organs by HPLC. In Figures 5B,

5C, and 5D, (L+) represented that only the tumor site was irradiated with 660-nm light (0.2 W/cm^2, 30 min) at 2 h post-injection, the other tissues was not received.

Once circulating in the tumor interstitium, the 660-nm light irradiation should induce the PEG deshielding from TK-$NP_{Ce6\&PTX}$, resulting in the enhanced tumor cell uptake and consequently improving the tumor accumulation. To verify this speculation, mice with MDA-MB-231 xenografts were administered ^{FITC}TK-$NP_{Ce6\&PTX}$, $^{FITC}NP_{Ce6\&PTX}$ or free PTX, and the tumor sites were irradiated with 660-nm light (0.2 W/cm^2, 30 min) at 2 h post-injection. At 6 h or 24 h post-injection, the mice were sacrificed to collect the tumor tissue and main organs. Subsequently, the PTX content in the tumor tissue was quantified using HPLC, and the tumor accumulation of both FITC-labeled nanocarriers was visualized using a Xenogen IVIS® Lumina system. Figure 5B shows that the PTX contents in the tumor tissue after 6 h and 24 h administration of ^{FITC}TK-$NP_{Ce6\&PTX}$ plus 660-nm light irradiation (^{FITC}TK-$NP_{Ce6\&PTX}$(L+)) were 1.37-fold and 1.55-fold higher than the amount that accumulated without light irradiation (^{FITC}TK-$NP_{Ce6\&PTX}$(L-)), respectively. In contrast, for the $^{FITC}NP_{Ce6\&PTX}$ groups, the PTX content in the tumor tissue was almost not affected by the light irradiation, exhibiting a similar level to the ^{FITC}TK-$NP_{Ce6\&PTX}$(L-) group. Meanwhile, the result generated by the Xenogen IVIS® Lumina system further indicated that the highest FITC fluorescent signal in the tumor tissue was visualized in the ^{FITC}TK-$NP_{Ce6\&PTX}$(L+) group in comparison to ^{FITC}TK-$NP_{Ce6\&PTX}$(L-) (Figure 5C). Such enhanced tumor accumulation under 660-nm laser irradiation was not found in the mice injected with $^{FITC}NP_{Ce6\&PTX}$. It should be noted that the enhanced PTX accumulation was not observed in the other organs (Figure 5D) because the PEG shielding was not realized in the absence of 660-nm light irradiation. Thus, the high PEGylation potentially reduced nonspecific cellular uptake by normal healthy cells, which consequently avoided cytotoxicity to normal tissues or organs.

The above results demonstrated that the high degree of PEGylation ensured the significantly prolonged circulation of TK-$NP_{Ce6\&PTX}$ in the blood, while the photoinduced PEG deshielding in the tumor tissue efficiently enhanced the cellular uptake by tumor cells and improved the PTX accumulation in tumor tissue, which could elevate the anticancer efficacy of TK-$NP_{Ce6\&PTX}$ plus light irradiation. To demonstrate this, mice bearing MDA-MB-231 tumors were intravenously injected with TK-$NP_{Ce6\&PTX}$, $NP_{Ce6\&PTX}$ or free PTX in 1% DMSO, and a portion of each group was irradiated with a 660-nm laser (0.2 W/cm^2, 30 min) at 2 h post-injection. As indicated in Figure 6A, treatment with TK-$NP_{Ce6\&PTX}$ and $NP_{Ce6\&PTX}$ only moderately inhibited tumor growth, and there were no significant differences among the formulations. The 660-nm light irradiation slightly improved the anticancer efficacy of $NP_{Ce6\&PTX}$, which could be due to the photodynamic effect of the encapsulated Ce6. In contrast, the growth of the tumor was most efficiently suppressed in the TK-$NP_{Ce6\&PTX}$ group with light irradiation (TK-$NP_{Ce6\&PTX}$(L+)), which verified that the photoinduced PEG deshielding significantly enhanced anticancer efficacy of TK-$NP_{Ce6\&PTX}$ due to the enhanced cellular uptake. It should be noted that there is no obvious body weight loss during treatment with these formulations (Figure S8), suggesting the negligible toxicities of these treatments. In addition, inspection of the tumor pictures of all formulations in Figure 6B further supported the above conclusion that the TK-$NP_{Ce6\&PTX}$(L+) group exhibited the highest anticancer efficiency. Moreover, an evaluation of the tumor growth rates (Figure 6C) and the tumor weights (Figure 6D) among all the formulations also indicated that the TK-$NP_{Ce6\&PTX}$(L+) group exhibited the greatest improvement in antitumor efficiency.

Finally, immunohistochemical staining was used to analyze cell proliferation and apoptosis in the tumor tissues after treatment. As shown in Figure 6E, treatment with TK-$NP_{Ce6\&PTX}$(L+) more efficiently reduced the percentage of proliferating PCNA-positive tumor cells (proliferating

cells) and increased the percentage of TUNEL-positive tumor cells (apoptotic cells), further confirming that the photoinduced PEG deshielding effect at the tumor site realized superior anticancer efficacy of the nanocarrier.

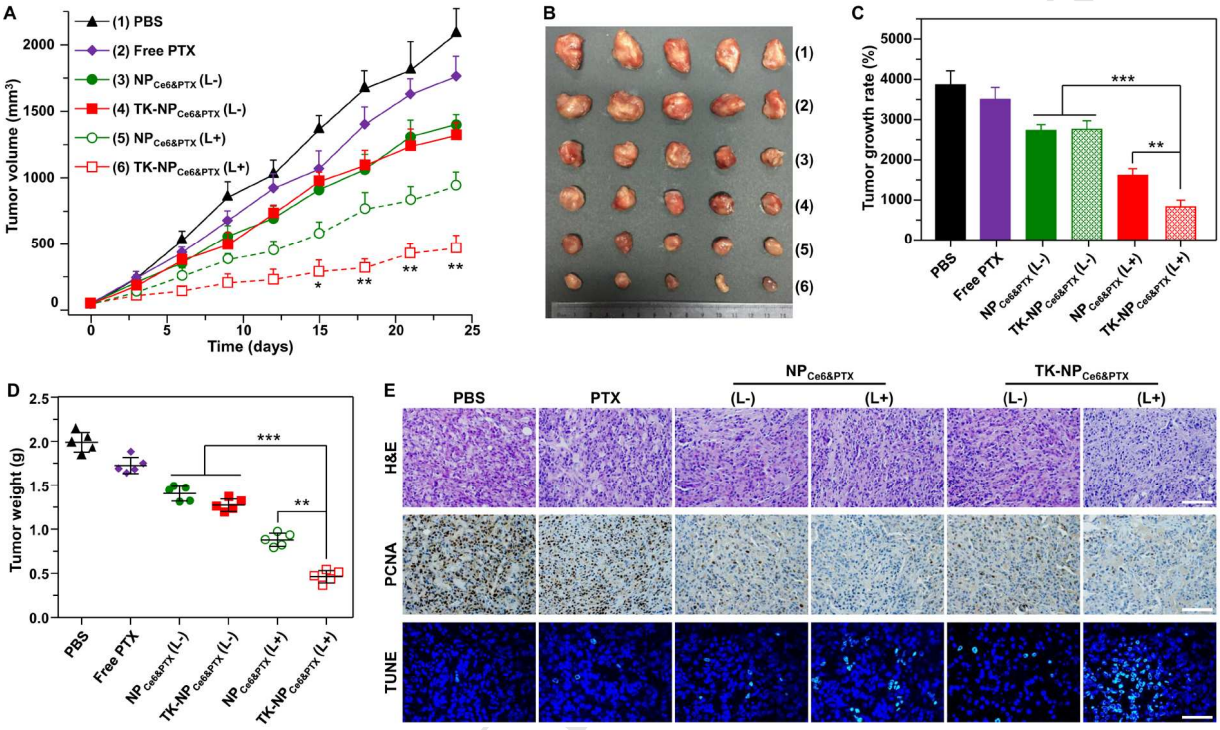

Figure 6. Photoinduced PEG deshielding for elevated anticancer efficacy *in vivo*. (A) The MDA-MB-231 tumor growth curves (A) of PBS, free PTX in 1% DMSO, TK-$NP_{Ce6\&PTX}$, and $NP_{Ce6\&PTX}$ after intravenous administration. (B, C, D) Tumor images (B), tumor growth rates (C) and tumor weights (D) of various groups at the last time point of measurement. (L+) and (L-) represent whether the tumor sites were irradiated with 660-nm light (0.2 W/cm^2, 30 min) at 2 h post-injection. (E) The H&E, PCNA and TUNEL analyses of tumor tissues after treatment. The scale bar is 50 μm. *$p < 0.05$; **$p < 0.01$; **$p < 0.005$.

4. CONCLUSION

We have successfully constructed an innovative nanocarrier TK-$NP_{Ce6\&PTX}$ with photoinduced PEG deshielding capability through designing bridged PEG and PLA copolymers with an ROS-sensitive TK linker. Under 660-nm light irradiation, the TK linker was efficiently cleaved by the encapsulated Ce6-generated ROS *in situ*. Then, the PEG corona detached from the nanocarriers. As a result of the specifically photoinduced PEG deshielding in the tumor tissue, enhanced cellular uptake and improved antitumor efficacy were realized in comparison with the conventional mPEG-*b*-PLA nanocarrier. This strategy could be extended to on-demand drug delivery to a variety of desired tissues and cells, providing a precisely and remotely controlled drug delivery approach.

Conflict of Interest

The authors declare no competing financial interest.

Acknowledgements

This work was supported by the National Key R&D Program of China (2017YFA0205601), and National Natural Science Foundation of China (51473043, 51390482, 51773067, 51603150), the Natural Science Foundation for Distinguished Young Scholars of Guangdong Province (2017B030306002), and the Fundamental Research Funds for the Central Universities.

References

[1] N.J. Butcher, G.M. Mortimer, R.F. Minchin, Unravelling the stealth effect, Nat. Nanotechnol. 11 (2016) 310-311.

[2] A. Kolate, D. Baradia, S. Patil, I. Vhora, G. Kore, A. Misra, PEG - A versatile conjugating

ligand for drugs and drug delivery systems, J. Controlled Release 192 (2014) 67-81.

[3] G. Pasut, F.M. Veronese, State of the art in PEGylation: The great versatility achieved after forty years of research, J. Controlled Release 161 (2012) 461-472.

[4] J.S. Suk, Q. Xu, N. Kim, J. Hanes, L.M. Ensign, PEGylation as a strategy for improving nanoparticle-based drug and gene delivery, Adv. Drug Delivery Rev. 99 (2016) 28-51.

[5] S. Schoettler, G. Becker, S. Winzen, T. Steinbach, K. Mohr, K. Landfester, et al., Protein adsorption is required for stealth effect of poly(ethylene glycol)- and poly(phosphoester)-coated nanocarriers, Nat. Nanotechnol. 11 (2016) 372-377.

[6] Z.Y. Poon, D.S. Chang, X.Y. Zhao, P.T. Hammond, Layer-by-layer nanoparticles with a pH-sheddable layer for in vivo targeting of tumor hypoxia, ACS Nano 5 (2011) 4284-4292.

[7] Q.H. Sun, Z.X. Zhou, N.S. Qiu, Y.Q. Shen, Rational design of cancer nanomedicine: nanoproperty integration and synchronization, Adv. Mater. 29 (2017) 1606628

[8] H.J. Zou, Z.J. Wang, M. Feng, Nanocarriers with tunable surface properties to unblock bottlenecks in systemic drug and gene delivery, J. Controlled Release 214 (2015) 121-133.

[9] D. Peer, J.M. Karp, S. Hong, O.C. FaroKhzad, R. Margalit, R. Langer, Nanocarriers as an emerging platform for cancer therapy, Nat. Nanotechnol. 2 (2007) 751-760.

[10] Y. Lu, A.A. Aimetti, R. Langer, Z. Gu, Bioresponsive materials, Nat. Rev. Mater. (2016) 16075

[11] R. Cheng, F.H. Meng, C. Deng, Z.Y. Zhong, Bioresponsive polymeric nanotherapeutics for targeted cancer chemotherapy, Nano Today 10 (2015) 656-670.

[12] Y.Q. Xia, J. Tian, X.Y. Chen, Effect of surface properties on liposomal siRNA delivery, Biomaterials 79 (2016) 56-68.

[13] B. Pelaz, P. Del Pino, P. Maffre, R. Hartmann, M. Gallego, S. Rivera-Fernandez, et al., Surface functionalization of nanoparticles with polyethylene glycol: Effects on protein adsorption and cellular uptake, ACS Nano 9 (2015) 6996-7008.

[14] M.M. Fan, Y. Zeng, H.T. Ruan, Z.R. Zhang, T. Gong, X. Sun, Ternary nanoparticles with a sheddable shell efficiently deliver microRNA-34a against CD44-positive melanoma, Mol. Pharmaceutics 14 (2017) 3152−3163

[15] H. Hatakeyama, H. Akita, H. Harashima, A multifunctional envelope type nano device (MEND) for gene delivery to tumours based on the EPR effect: A strategy for overcoming the PEG dilemma, Adv. Drug Delivery Rev. 63 (2011) 152-160.

[16] S. Hama, S. Itakura, M. Nakai, K. Nakayama, S. Morimoto, S. Suzuki, et al., Overcoming the polyethylene glycol dilemma via pathological environment-sensitive change of the surface property of nanoparticles for cellular entry, J. Controlled Release 206 (2015) 67-74.

[17] W. Zhang, Q. Cheng, S. Guo, D. Lin, P. Huang, J. Liu, et al., Gene transfection efficacy and biocompatibility of polycation/DNA complexes coated with enzyme degradable PEGylated hyaluronic acid, Biomaterials 34 (2013) 6495-6503.

[18] X.Z. Yang, J.Z. Du, S. Dou, C.Q. Mao, H.Y. Long, J. Wang, Sheddable ternary nanoparticles for tumor acidity-targeted siRNA delivery, ACS Nano 6 (2012) 771-781.

[19] C.F. Xu, H.B. Zhang, C.Y. Sun, Y. Liu, S. Shen, X.Z. Yang, et al., Tumor acidity-sensitive linkage-bridged block copolymer for therapeutic siRNA delivery, Biomaterials 88 (2016) 48-59.

[20] H.X. Wang, X.Z. Yang, C.Y. Sun, C.Q. Mao, Y.H. Zhu, J. Wang, Matrix metalloproteinase 2-responsive micelle for siRNA delivery, Biomaterials 35 (2014) 7622-7634.

[21] F. Fan, Y. Yu, F. Zhong, M. Gao, T.M. Sun, J.X. Liu, et al., Design of tumor acidity-responsive sheddable nanoparticles for fluorescence/magnetic resonance imaging-guided photodynamic therapy, Theranostics 7 (2017) 1290-1302.

[22] X.Z. Yang, X.J. Du, Y. Liu, Y.H. Zhu, Y.Z. Liu, Y.P. Li, et al., Rational design of polyion complex nanoparticles to overcome cisplatin resistance in cancer therapy, Adv. Mater. 26 (2014) 931-936.

[23] P.L. Bedard, A.R. Hansen, M.J. Ratain, L.L. Siu, Tumour heterogeneity in the clinic. Nature 501 (2013) 355-364.

[24] M.R. Junttila, F.J. De Sauvage, Influence of tumour micro-environment heterogeneity on therapeutic response, Nature 501 (2013) 346-354.

[25] S. Wang, P. Huang, X.Y. Chen, Stimuli-responsive programmed specific targeting in nanomedicine, ACS Nano 10 (2016) 2991-2994.

[26] L. Cheng, C. Wang, L.Z. Feng, K. Yang, Z. Liu, Functional nanomaterials for phototherapies of cancer, Chem. Rev. 114 (2014) 10869-10939.

[27] D.D. Li, Y.C. Ma, J.Z. Du, W. Tao, X.J. Du, X.Z. Yang, et al., Tumor acidity/NIR controlled interaction of transformable nanoparticle with biological systems for cancer therapy, Nano Lett. 17 (2017) 2871-2878.

[28] G.B. Yang, X.Q. Sun, J.J. Liu, L.Z. Feng, Z. Liu, Light-Responsive, Singlet-oxygen-triggered on-demand drug release from photosensitizer-doped mesoporous silica nanorods for

cancer combination therapy, Adv. Funct. Mater. 26 (2016) 4722-4732.

[29] D.D. Li, G.B. Zhang, W.G. Xu, J.X. Wang, Y.C. Wang, L.Z. Qiu, et al., Investigating the effect of chemical structure of semiconducting polymer nanoparticle on photothermal therapy and photoacoustic imaging, Theranostics 7 (2017) 4029-4040.

[30] J.J. Hu, Q. Lei, M.Y. Peng, D.W. Zheng, Y.X. Chen, X.Z. Zhang, A positive feedback strategy for enhanced chemotherapy based on ROS-triggered self-accelerating drug release nanosystem, Biomaterials 128 (2017) 136-146.

[31] L.H. Liu, W.X. Qiu, L. Bin, C. Zhang, L.F. Sun, S.S. Wan, et al., A red light activatable multifunctional prodrug for image-guided photodynamic therapy and cascaded chemotherapy, Adv. Funct. Mater. 26 (2016) 6257-6269.

[32] F.Y. Zhou, B. Feng, T.T. Wang, D.G. Wang, Z.R. Cui, S.L. Wang, et al., Theranostic prodrug vesicles for reactive oxygen species-triggered ultrafast drug release and local-regional therapy of metastatic triple-negative breast cancer, Adv. Funct. Mater. 27 (2017) 1703674.

[33] C.X. Yue, Y.M. Yang, C.L. Zhang, G. Alfranca, S.L. Cheng, L.J. Ma, et al., ROS-responsive mitochondria-targeting blended nanoparticles: chemo-and photodynamic synergistic therapy for lung cancer with on-demand drug release upon irradiation with a single light source, Theranostics 6 (2016) 2352-2366.

[34] X. Xu, P.E. Saw, W. Tao, Y. Li, X. Ji, S. Bhasin, et al., ROS-responsive polyprodrug nanoparticles for triggered drug delivery and effective cancer therapy, Adv. Mater. 29 (2017) 1700141.

[35] R. Sun, X.J. Du, C.Y. Sun, S. Shen, Y. Liu, X.Z. Yang, et al., A block copolymer of zwitterionic polyphosphoester and polylactic acid for drug delivery, Biomater. Sci. 3 (2015) 1105-1113.

[36] Z. Cao, Y. Ma, C. Sun, Z. Lu, Z. Yao, J. Wang, et al., ROS-sensitive polymeric nanocarriers with red light-activated size shrinkage for remotely controlled drug release, Chem. Mater. 30 (2018) 517-525.

[37] T.M. Sun, J.Z. Du, Y.D. Yao, C.Q. Mao, S. Dou, S.Y. Huang, et al., Simultaneous delivery of siRNA and paclitaxel via a "Two-in-One" micelleplex promotes synergistic tumor suppression, ACS Nano 5 (2011) 1483-1494.

[38] F. Brandl, N. Bertrand, E. M. Lima, R. Langer, Nanoparticles with photoinduced precipitation for the extraction of pollutants from water and soil, Nat. Commun. 6 (2015) 7765.

[39] C.Y. Sun, Y. Liu , J.Z. Du, Z.T. Cao, C.F. Xu, J. Wang, Facile generation of tumor pH-labile linkage-bridged block copolymer for expeditious chemotherapeutic delivery, Angew. Chem. Int. Edit. 128 (2016) 1010-1014.

[40] X.J. Du, J.L. Wang, W.W. Liu, J.X. Yang, C.Y. Sun, R. Sun, et al., Regulating the surface poly(ethylene glycol) density of polymeric nanoparticles and evaluating its role in drug delivery in vivo, Biomaterials 69 (2015)1-11.

[41] J.L. Perry, K.G. Reuter, M.P. Kai, K.P. Herlihy, S.W. Jones, J.C. Luft, et al., PEGylated PRINT nanoparticles: the impact of PEG density on protein binding, macrophage association, biodistribution, and pharmacokinetics, Nano Lett. 12 (2012) 5304-5310.

Graphical Table of Contents